Nonlinear PI Control for Variable Pitch Wind Turbine

Yaxing Ren[a], Liuying Li[a], Joseph Brindley[b], Lin Jiang[a,*]

[a] *Department of Electronics and Electrical Engineering, University of Liverpool, Brownlow Hill, Liverpool, L69 3GJ, United Kingdom*
[b] *Gencoa Ltd., Physics Road, Liverpool, L24 9HP, United Kingdom*

Abstract

Wind turbine uses a pitch angle controller to reduce the power captured above the rated wind speed and release the mechanical stress of the drive train. This paper investigates a nonlinear PI (N-PI) based pitch angle controller, by designing an extended-order state and perturbation observer to estimate and compensate unknown time-varying nonlinearities and disturbances. The proposed N-PI does not require the accurate model and uses only one set of PI parameters to provide a global optimal performance under wind speed changes. Simulation verification is based on a simplified two-mass wind turbine model and a detailed aero-elastic wind turbine simulator (FAST), respectively. Simulation results show that the N-PI controller can provide better dynamic performances of power regulation, load stress reduction and actuator usage, comparing with the conventional PI and gain-scheduled PI controller, and better robustness against of model uncertainties than feedback linearization control.

Keywords: Nonlinear PI, Extended-order State and Perturbation Observer, Pitch angle control, Wind turbines, FAST

2015 MSC: 00-01, 99-00

*This project is part funded by the European Regional Development Fund via Centre for Global Eco-Innovation, and part by EPSRC Grant (EP/J014249/1). Corresponding author: Lin Jiang, Tel.: +44-151-794-4509; Fax: +44-151-794 4540; E-mail: ljiang@liverpool.ac.uk.

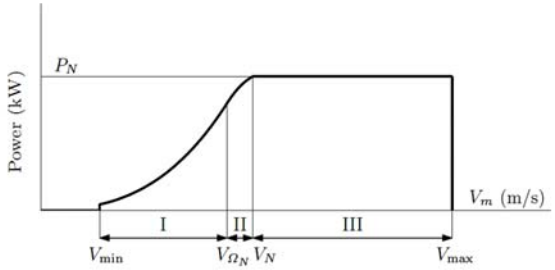

Figure 1: Wind turbine operation modes versus wind speed [1]

1. Introduction

Wind power is one of the most promising renewable energy sources and has received tremendous progress at the past decade. Most wind power generation system uses variable speed wind turbine with variable pitch to achieve an efficient and reliable conversion of wind power to electrical power. According to wind speed range, wind turbine has three operation modes and control objectives, as shown in Figure 1 [1]. Region I starts from the cut-in wind speed to wind speed when the rotor speed reaches its rated value and its' control objective is to capture the maximum available power from the wind flow, using variable speed operation of wind turbine [2]. In region III, the wind speed is above its rated value and below the cut-out speed, in which the wind power forced on the blade is larger than the nominal power of the wind turbine and must be limited by pitch angle control, while minimizing the load stress on drive-train shaft at the same time. Between these two regions, the rotor speed can reach its rated value and must be kept constant until the generated power reaches the rated power. This buffer region is called Region II, whose control objective is to smoothly connect Region I and III [3].

Efficient and reliable operation of a WPGS heavily relies on the control systems applied on the WT operating at different regions. At the high speed region III, pitch angle control is applied to limit the wind power captured by the wind turbine. Numerous control methods have been applied to design pitch angle controllers to, such as PI-type controller [1][4]. The wind turbine is a

highly non-linear system due to its nonlinear aerodynamics [5][6]. As the wind turbine contains strong aerodynamic nonlinearities and operates under time-varying wind power inputs, the linear PI with fixed gains cannot provide consistently satisfactory performance in the whole wind speed region. Advanced control methodologies have been applied to tackle this problem, such as the gain scheduling PI (GSPI) [1][4], digital robust control [7], neural-network-based control [8], model predictive control [9], and feedback linearization control [10][6]. However, most control methods, such as the feedback linearization control, are designed based on the accurate wind turbine model, which is difficult to be obtained accurately in practical.

Extended-order state and perturbation (or disturbance) observer (ESPO) has been proposed to estimate system state and perturbation term for nonlinear system which can be represented as an chained-integrator system and matched nonlinearities and disturbances. By defining perturbation as a lumped term to include all unknown nonlinearities, parameter uncertainties and external disturbance [11], ESPO can be implemented using nonlinear observer [12][13][14], linear observers [15][16], sliding mode observers [17], fuzzy observers [18], and neural-network-based observers [19]. ESPO-based controller use the estimate of perturbation to compensate its real perturbation and achieve the adaptive feedback linearizing control, without requiring a detailed and accurate system model in conventional feedback linearization (FL) control [10][6]. They have been applied in robotic systems [20], power systems [15][21], PMSM systems [11], induction motor [22], doubly-fed induction generator wind turbine [23].

This paper designs a Nonlinear PI (N-PI) controller for wind turbine pitch angle control. It consists of an ESPO and a classic PI controller. The ESPO is used to estimate the unknown time-varying nonlinearities and disturbance, which are defined in a lumped perturbation term. The N-PI uses the estimated perturbation to compensate the real one for linearizing the nonlinear system. The procedure is similar to the feedback linearization (FL) method, which requires a detailed and accurate system model to calculate the nonlinearities [6][10]. The N-PI is proposed to provide global and consistent optimal

performance across the whole operation range only based on one set of PI gains tuned around the mean wind speed, and avoid the rapidly switching of gains of the gain-scheduled PI (GSPI) type controllers. Two types of gain scheduled PI controllers, wind speed switching and pitch-angle switching ones are compared using simulation tests based on simplified two mass model and a detailed aero-elastic wind turbine simulator, FAST [24].

2. Nonlinear Wind Turbine Modeling

The configuration of a simplified two-mass model of wind turbine and its nonlinear power coefficient C_p is shown in Figure 2. The model is presented in a generalized nonlinear form as follows [26]:

$$\dot{\mathbf{x}} = \mathbf{F}(\mathbf{x}) + \mathbf{B}u = \begin{bmatrix} f_1 \\ f_2 \\ f_3 \\ f_4 \end{bmatrix} + \begin{bmatrix} 0 \\ 0 \\ 0 \\ g_4 \end{bmatrix} u \tag{1}$$

The state vector $\mathbf{x}$, control input u and nonlinear vector $\mathbf{F}(\mathbf{x})$ are defined as:

$$\begin{aligned} \mathbf{x} &= [\omega_r \quad \omega_g \quad \delta \quad \beta]^T \\ u &= \beta_r \end{aligned} \tag{2}$$

$$\mathbf{F}(\mathbf{x}) = \begin{bmatrix} f_1 \\ f_2 \\ f_3 \\ f_4 \end{bmatrix} = \begin{bmatrix} \frac{P_r(x_1,x_4,V)}{x_1 J_r} - \frac{x_1 D_s}{J_r} + \frac{x_2 D_s}{N_g J_r} - \frac{x_3 K_s}{J_r} \\ \frac{x_1 D_s}{N_g J_g} - \frac{x_2 D_s}{N_g^2 J_g} + \frac{x_3 K_s}{N_g J_g} - \frac{T_g}{J_g} \\ x_1 - \frac{x_2}{N_g} \\ -\frac{1}{\tau_\beta} x_4 \end{bmatrix} \tag{3}$$

$$\mathbf{B} = \begin{bmatrix} 0 & 0 & 0 & g_4 \end{bmatrix}^T$$

$$g_4 = \frac{1}{\tau_\beta}$$

where ω_r is rotor speed, ω_g is generator speed, δ is twist angle, and β is pitch angle. τ_β is time constants of pitch actuator, and β_r is the pitch angle control.

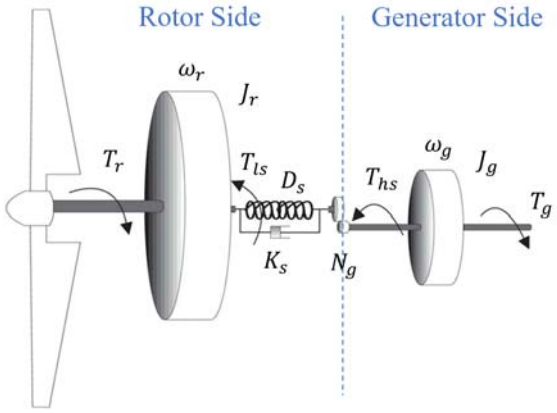

(a)

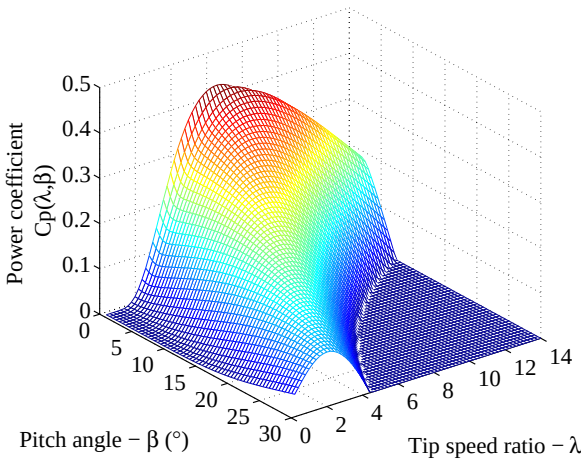

(b)

Figure 2: Two-mass variable speed wind turbine model and nonlinear power coefficient Cp [25]

T_g is generator torque, J_r and J_g are rotor and generator inertia, N_g is gear ratio, D_s and K_s are drive-train damping and spring constant, respectively.

The mechanical power P_r captured by the wind turbine is:

$$P_r = \frac{1}{2}\pi\rho R^2 V^3 C_p(x_1, x_4, V) \tag{4}$$

where R is the rotor radius, ρ is the air density, V is the wind speed. C_p is the power conversion coefficient of wind turbine and is a nonlinear function of β and λ. This paper uses Controls Advanced Research Turbine (CART) located at National Renewable Energy Laboratory USA and its function is given as [5]:

$$C_p = 0.22(116\lambda_t - 0.4x_4 - 5)e^{-12.5\lambda_t} \tag{5}$$

where

$$\lambda_t = \frac{1}{\lambda + 0.08\beta} - \frac{0.035}{\beta^3 + 1}$$
$$\lambda = \frac{\omega_r R}{V}$$

where λ is tip-speed ratio and λ_t is a intermediate variable.

Control objective of this paper is to design a nonlinear pitch angle control for wind turbine operating at Region III, using limiting the power captured by the wind turbine to maintain the rotor rotation speed ω_r, or the system output power P_e, at its rated value.

3. Conventional PI and Gain-scheduled PI Controller

3.1. PI Controller

The conventional PI(D) based pitch angle controller is used to regulate the rotor speed or the output power of wind turbine [4]. To get the optimal control gain under the rated operating point, particle swarm optimization (PSO) method is used [27][28]. The integral time absolute error (ITAE) of rotor speed is used as the optimization objective and defined as

$$ITAE = \int_0^\infty t|e(t)|dt \tag{6}$$

The PSO method is implemented following the reference [27][28]. The the velocity for searching a new best position of each swarm in PSO is given as:

$$\begin{aligned} v = \quad & w \cdot v + c_1 \cdot \mathrm{rand}(2, N) \times (P_{\mathrm{l,best}} - P_{\mathrm{current}}) \\ & + c_2 \cdot \mathrm{rand}(2, N) \times (P_{\mathrm{g,best}} - P_{\mathrm{current}}) \end{aligned}$$

where N is the number of units, M is the maximum number of swim length, w is the momentum or inertia of PSO, $P_{\mathrm{l,best}}$ is the local best position, $P_{\mathrm{g,best}}$ is the global best position, and P_{current} is the current position; $\mathrm{rand}(2, N)$ is to generate a $2 \times N$ matrix with random values, c_1 and c_2 are the coefficient for random values. The special parameters of PSO used in this paper are given as $N = 50$, $M = 20$, $w = 0.9$, $c_1 = 0.12$ and $c_2 = 1.2$.

Control gains of the PI controller is optimized at the nominal operation point under mean wind speed, where $V_0 = 18$ m/s, $\omega_{r0} = 2.1428$ rad/s, and $\beta_0 = 25°$. The optimized gains of the PI pitch controller are $k_p = 140$ and $k_i = 52$, respectively.

3.2. Gain Scheduled PI Controller

Due to the high aerodynamic nonlinearities of wind turbine and time-varying wind speed, the PI controller using one set of gains optimized based on one operation point cannot provide consistent optimal performance when operation points shifts from that normal point. To tackle this problem, gain scheduled PI pitch control has been proposed [1].

3.2.1. Wind-speed Based Switching

A GSPI controller requires the wind speed measuremeasent to schedule the controller gains [26]. An anemometer can be used but it can only measure the wind speed at a special point, which is not accurate for representing the effective wind speed in large wind turbines. To achieve a more accurate estimation of the effective wind speed, the wind turbine itself can be used as a sensor and the estimation can be solved by Newton-Raphson method [6].

The wind speed estimator is realized by minimizing the cost function $J(t, V)$

$$J(t, V) = \left(P_r(t) - f_r(V)\right)^2 \tag{7}$$

$$f_r(V) = \frac{1}{2}\pi\rho R^2 V^3 C_p(\beta, \lambda) \tag{8}$$

where $P_r(t)$ is a measurement of rotor power at time t, which is assumed known; $f_r(V)$ is the aerodynamic power function of wind speed V.

The problem is equivalent to find the solution of

$$I(t, V) = P_r(t) - \frac{1}{2}\pi\rho R^2 V^3 C_p(\beta, \lambda) = 0 \tag{9}$$

From the partial derivative equation

$$\Delta P_r = \frac{\partial P_r}{\partial V}\Delta V \tag{10}$$

the iteration form of the estimator can be written as:

$$\widehat{V} = \Delta P_r \left(\frac{\partial P_r}{\partial V}\right)^{-1} \tag{11}$$

where

$$\frac{\partial P_r}{\partial V} = -\frac{3}{2}\pi\rho R^2 V^2 C_p(\beta, \lambda) - \frac{1}{2}\pi\rho R^2 V^3 \frac{\partial C_p}{\partial V}$$

$$\frac{\partial C_p}{\partial V} = -\frac{0.22}{\omega_r R}\frac{178.5 - 1450\lambda_t + 5x_4}{(\lambda + 0.08x_4)^2} e^{-12.5\lambda_t}$$

At time t, using the measured rotor power $P_r(t)$, the iteration will be performed until

$$I(t, \hat{V}_t) = P_r(t) - f_r(\hat{V}_t) < \varepsilon \tag{12}$$

where ε is a small value. The estimation of wind speed at time t is then $\hat{V}_t$.

Since the rotor power P_r is unmeasurable in practice, the assumption is made that the rotor power is equal to electrical power P_e, which is measurable, divided by the wind turbine power conversion efficiency η. Then the estimated wind speed can be used in the GSPI controller to switching the scheduled gains by look-up-table for the pitch controller.

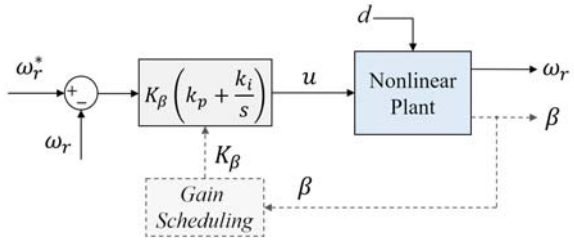

(a)

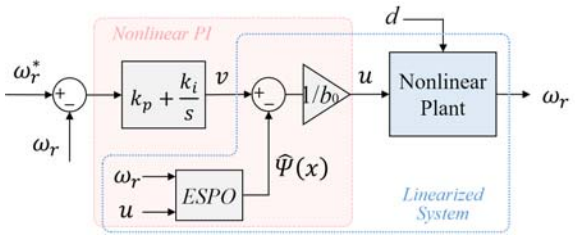

(b)

Figure 3: Block diagram of (a) conventional PI or gain-scheduling PI (GS PI) controller, (b) proposed Nonlinear PI (N-PI) controller.

3.2.2. Pitch-angle Based Switching

As wind speed based switching requires a complex estimation of the real-time wind speed and also may result in fast switching between gains due to the fast change of wind speed, an improved GSPI based on pitch angle switching has been proposed [29][30][31]. The control block diagram of the PI and gain-scheduled PI controller is shown in Figure 3(a), where the K_β is set to be 1 in the PI controller. Under different wind speeds, optimal gains are obtained using the PSO method with the performance index of ITAE. The optimal gains of k_p and k_i under different wind speed and the correspondent pitch angle are given in Table 1.

To obtain a continuous pitch angle based switching, the scheduled gain pairs are obtained as the product of a constant PI gain pair multiplied by a scheduled gain $K(\beta)$ which is a function of pitch angle [30]. The scheduled gain $K(\beta)$ is proposed to compensate the variation of the aerodynamic sensitivity, $\partial P_r/\partial\beta$,

Table 1: Optimal Gains under Corresponding Wind Speed and Pitch Angle using PSO Optimization Method

V (m/s)	$\beta_{rated}(^\circ)$	$k_{\mathrm{p,opt}}(^\circ\cdot\mathrm{s/rad})$	$k_{i,opt}(^\circ\cdot\mathrm{s}^2/\mathrm{rad})$
12	3.6	186	70
14	14.1	178	66
16	20.6	160	60
18	25.1	140	52
20	28.6	124	46

and is obtained using the trend line of the optimal gains versus pitch angle is given as [30]

$$u = K(\beta)\left(k_p + \frac{k_i}{s}\right)(x_1 - \omega_r^*) \tag{13}$$

where

$$K(\beta) = \begin{cases} 1.6, & \text{for} \quad -1^\circ < \beta \leq 0^\circ \\ -0.001\beta^2 + 0.01\beta + 1.6, & \text{for} \quad 0^\circ < \beta \leq 30^\circ \\ 1, & \text{for} \quad \beta > 30^\circ \end{cases} \tag{14}$$

and the constant proportional and integral gains, $k_p = 116$, and $k_i = 42$.

4. ESPO-based Nonlinear PI Pitch Angle Controller

4.1. Input-output Linearization

The input-output relationship between the system output, the rotor speed as $y = x_1$, and the system input, the pitch angle control as $u = \beta_r$, can be obtained using differentiating the output till the control input appearing. From system (1)-(3), the rotor speed dynamic is given as:

$$\dot{x}_1 = \frac{P_r(x_1, x_4, V)}{x_1 J_r} - \frac{x_1 D_s}{J_r} + \frac{x_2 D_s}{N_g J_r} - \frac{x_3 K_s}{J_r} \tag{15}$$

Its second-order derivative can be obtained as

$$\frac{d^2 x_1}{dt^2} = L_f(x) + L_g(x)u \tag{16}$$

where

$$L_f(x) = \sum_{i=1}^{4} \left(\frac{\partial f_1}{\partial x_i} \cdot f_i \right) + \frac{\partial f_1}{\partial V} \cdot \dot{V}$$

$$\frac{\partial f_1}{\partial x_1} = -\frac{1}{J_r x_1} \left[\frac{P_r}{x_1} + 0.11\pi\rho R^3 V^2 \frac{178.5 - 1450\lambda_t + 5x_4}{(\lambda + 0.08x_4)^2} e^{-12.5\lambda_t} \right] - \frac{D_s}{J_r}$$

$$\frac{\partial f_1}{\partial x_2} = \frac{D_s}{N_g J_r}$$

$$\frac{\partial f_1}{\partial x_3} = -\frac{K_s}{J_r}$$

$$\frac{\partial f_1}{\partial x_4} = \frac{0.11\pi\rho R^2 V^3}{x_1 J_r} \left\{ (178.5 - 1450\lambda_t + 5x_4) \left[\frac{-0.08}{(\lambda + 0.08x_4)^2} + \frac{0.105x_4^2}{(x_4^3 + 1)^2} \right] - 0.4 \right\} e^{-12.5\lambda_t}$$

$$\frac{\partial f_1}{\partial V} = \frac{0.11\pi\rho R^3 V}{J_r(\lambda + 0.08x_4)^2} (178.5 - 1450\lambda_t + 5x_4) e^{-12.5\lambda_t}$$

$$L_g(x) = \frac{\partial f_1}{\partial x_4} g_4$$

$$= \frac{0.11\pi\rho R^2 V^3}{x_1 J_r \tau_\beta} \left\{ (178.5 - 1450\lambda_t + 5x_4) \left[\frac{-0.08}{(\lambda + 0.08x_4)^2} + \frac{0.105x_4^2}{(x_4^3 + 1)^2} \right] - 0.4 \right\} e^{-12.5\lambda_t}$$

where $\dot{V}$ is the derivative of wind speed.

When nonlinearities $L_f(x)$ and system input gain $L_g(x)$, and wind speed dynamic $\dot{V}$ are known, a feedback linearized control (FLC) can be obtained as

$$u = \frac{1}{L_g(x)} \left(v - L_f(x) \right) \tag{17}$$

where $L_g(x) \neq 0$ for all operation points and v is the control of the linearized second-order system

$$\frac{d^2 x_1}{dt^2} = v \tag{18}$$

and is designed as PI-type controller in this paper, for the convenience of comparison with PI-type controller and GSPI controller.

4.2. Perturbation Definition and Extended-order State Space Model

Assume all nonlinearities represented as $L_f(x)$ and $L_g(x)$ in system (16) are unknown, define a perturbation term $\Psi(x)$ to include all system nonlinearities, and the time-varying wind dynamics as:

$$\Psi(x) = L_f(x) + \left(L_g(x) - b_0 \right) u \tag{19}$$

where $b_0 = L_g(x_0)$ is the nominal constant control gain which can be chosen as the mean value of $L_g(x)$. Then system (16) becomes

$$\frac{d^2x_1}{dt^2} = \Psi(x) + b_0 u \tag{20}$$

4.3. Extended-order States and Perturbation Observer

Define $z_1 = x_1$, $z_2 = \dot{x}_1$ and an additional state variable $z_3 = \Psi(x, z)$, an extended-order model is obtained as:

$$\begin{cases} \dot{z}_1 = z_2 \\ \dot{z}_2 = z_3 + b_0 u \\ \dot{z}_3 = \dot{\Psi}(x, t) \end{cases} \tag{21}$$

Define $\tilde{z}_1 = z_1 - \hat{z}_1$, a linear ESPO is designed as:

$$\begin{cases} \dot{\hat{z}}_1 = \hat{z}_2 + k_{01}\tilde{z}_1 \\ \dot{\hat{z}}_2 = \hat{z}_3 + b_0 u + k_{02}\tilde{z}_1 \\ \dot{\hat{z}}_3 = k_{03}\tilde{z}_1 \end{cases} \tag{22}$$

where $\hat{z}_i$, $i = 1, 2, 3$, is the estimate of z_i; and $\tilde{z}_1$ is the estimation error of z_1. k_{0i} are observer gains that can be parameterized as [22]:

$$[k_{01} \quad k_{02} \quad k_{03}] = \begin{bmatrix} 3\alpha_0 & 3\alpha_0^2 & \alpha_0^3 \end{bmatrix} \tag{23}$$

where α_0 is the observer bandwidth and the only parameter to be tuned.

Similarly, to improve the estimation performance, a nonlinear ESPO (NESPO) can also be designed based on [12] as follows:

$$\begin{cases} \dot{\hat{z}}_1 = \hat{z}_2 + k_{01}\tilde{z}_1 \\ \dot{\hat{z}}_2 = \hat{z}_3 + b_0 u + k_{02} fal(\tilde{z}_1, 0.5, h) \\ \dot{\hat{z}}_3 = k_{03} fal(\tilde{z}_1, 0.25, h) \end{cases} \tag{24}$$

$$fal(\chi, \sigma, h) = \begin{cases} \frac{\sigma^2}{h^{(1-\sigma)}}\chi & |\chi| \le h \\ \text{sign}(\chi) \cdot \sigma^2 |\chi|^\sigma & |\chi| > h \end{cases} \tag{25}$$

where χ is the input error of the nonlinear function, σ is the precision index from 0 to 1, h is the width of linear area of the nonlinear function.

Comparing with the linear ESPO, the NESPO can accelerate the estimation speed, with the cost of a complex nonlinear observer, which increases the difficulties of stability analysis of the closed-loop system. Note that other types of ESPO, such as sliding mode observer, can also been applied, though they all provide similar performance [15].

4.4. N-PI based Pitch Angle Controller

By using real-time estimate of perturbation $\hat{\Psi}(x)$ from the third-order ESPO to compensate the real perturbation, the control input u can be obtained as

$$u = \frac{1}{b_0}\left(v - \hat{\Psi}(x)\right) \tag{26}$$

where v is the control of the linearized second-order system and is designed as a classic PI controller with error between rotor speed reference ω_r^* and the system output x_1:

$$v = \left(k_p + \frac{k_i}{s}\right)(\omega_r^* - x_1) \tag{27}$$

Finally, the N-PI pitch angle control can be expressed as

$$u = \frac{1}{b_0}\left(k_p + \frac{k_i}{s}\right)(\omega_r^* - x_1) - \frac{1}{b_0}\hat{\Psi}(x) \tag{28}$$

The whole diagram of the N-PI pitch angle control is given in Figure 3(b). Note the N-PI controller uses only one pair of gains rather than several scheduled gain pairs like GSPI, due to the compensation of all system nonlinearities and disturbances.

4.5. Stability Analysis

Stability analysis of the observer (22) and the closed-loop system inlcuding controller and observer can be investigated by using Lyapunov stability similarly to [17]. Thus only stability results are summarized in this ppaer and detailed steps can follow [17]. Error dynamic of the observer can be obtained from system (21) and (22) as:

$$\begin{bmatrix} \dot{\tilde{z}}_1 \\ \dot{\tilde{z}}_2 \\ \dot{\tilde{z}}_3 \end{bmatrix} = \begin{bmatrix} -k_{01} & 1 & 0 \\ -k_{02} & 0 & 1 \\ -k_{03} & 0 & 0 \end{bmatrix} \begin{bmatrix} \tilde{z}_1 \\ \tilde{z}_2 \\ \tilde{z}_3 \end{bmatrix} + \begin{bmatrix} 0 \\ 0 \\ \dot{\Psi}(\cdot) \end{bmatrix} \tag{29}$$

Define tracking error of rotor speed as $e_2 = \omega_r^* - x_1$, its integration as $e_1 = \int_0^t (\omega_r^* - x_1)dt$, and its differentiation as $e_3 = \dot{\omega}_r^* - \dot{x}_1$. From (20) and (28), the dynamics of the closed-loop system is represented by the tracking errors as

$$\begin{bmatrix} \dot{e}_1 \\ \dot{e}_2 \\ \dot{e}_3 \end{bmatrix} = \begin{bmatrix} 0 & 1 & 0 \\ 0 & 0 & 1 \\ k_i & k_p & 0 \end{bmatrix} \begin{bmatrix} e_1 \\ e_2 \\ e_3 \end{bmatrix} + \begin{bmatrix} 0 \\ 0 \\ \tilde{z}_3 \end{bmatrix} \tag{30}$$

where $\tilde{z}_3 = \Psi(\cdot) - \hat{\Psi}(\cdot)$ is the estimation error of the perturbation.

Based on [17], assume perturbation functions $\Psi(\cdot)$ and $\dot{\Psi}(\cdot)$ are bounded over the domain of interest as:

$$|\Psi(\cdot)| \leq \gamma_1 \qquad |\dot{\Psi}(\cdot)| \leq \gamma_2 \tag{31}$$

where γ_1 and γ_2 are positive constants; then the error dynamic of ESPO (29) and the closed-loop system (30) are ultimately bounded. Furthermore, if perturbations $\Psi(\cdot)$ and $\dot{\Psi}(\cdot)$ are locally Lipschitz in their arguments, the observer error and the closed-loop tracking error can be obtained exponential converged as well.

The internal dynamic of the nonlinear system is analysed using zero-dynamic technique. When the rotor speed and its time derivative are well controlled, i.e. $e_2 = 0$ and $e_3 = 0$, then the corresponding states are controlled to their reference values, such as $\beta = \beta^*$, $\omega_r = \omega_r^*$, $\dot{\omega}_r = 0$ and $P_r(\omega_r^*, \beta^*) = P_r^* = P_e^*/\eta$, where η is the entire output power efficiency. A relation expression can be obtained as

$$\frac{P_r^*}{\omega_r^*} - \omega_r^* D_s + \frac{\omega_g D_s}{N_g} - \delta K_s = 0 \tag{32}$$

then the other two dynamics can be obtained as

$$\dot{\omega}_g \equiv 0 \tag{33}$$

$$\lim_{t \to \infty} \delta(t) = \frac{P_e^*/\eta}{\omega_r^* K_s} \tag{34}$$

The zero-dynamic of the internal system is stable, and therefore, the closed-loop system error dynamic is stable.

5. Simulation Results

The simulation tests were performed based on a real experimental wind turbine, Controls Advanced Research Turbine (CART) located at National Renewable Energy Laboratory USA and whose parameters are given in Table 2. The CART is a flexible, variable speed & pitch controlled wind turbine with 1.5 MW nominal power rating. This turbine was modeled using a two-mass model and a validated aeroelastic simulator called FAST: fatigue, aerodynamics, structures, and turbulence [24]. As only pitch angle control in Region III is considered, the wind speed is chosen in the range from 12 m/s to 24 m/s with different mean value and turbulence intensity. The wind parameters are generated from TurbSim, which is a stochastic, full-field, turbulent-wind simulator and numerically simulates 3-dimensional wind velocity vectors by time series at points in a vertical rectangular grid [32]. The proposed N-PI, a conventional PI

Table 2: Two-mass model parameters of the 1.5 MW experimental wind turbine.

Wind Turbine Parameters:	Value:
Rotor radius (R_{b})	35 m
Air density (ρ)	1.225 kg/m^3
Rotor inertia (J_{r})	2.96×10^6 kg·m^2
Generator inertia (J_{g})	53.0 kg·m^2
Drive-train spring factor (K_{s})	5.6×10^9 N·m/rad
Drive-train damping factor (D_{s})	1.0×10^7 N·m·s/rad
Gearbox ratio (N_{g})	87.965
Pitch actuator time constant (τ_β)	1 s
Nominal power output (P_{e})	1.5 MW
Rated rotor speed ($\omega_{\mathrm{r,rated}}$)	2.1428 rad/s
Rated generator torque ($T_{\mathrm{g,rated}}$)	8376.6 N·m
Pitch angle limit ($\beta_{\min} \sim \beta_{\max}$)	$-1^\circ \sim 90^\circ$
Pitch rate limit ($\dot{\beta}_{\lim}$)	$\pm10^\circ$/s
Wind turbine efficiency (η)	0.95

and a GSPI are tested based on the simplified two-mass model of the CART at first. The parameters of the N-PI controller are given in Table 3.

Table 3: Parameters of FLC and N-PI controller.

Parameters:	Value:
FLC/N-PI Proportional gain ($1/s^2$): k_p	6.3
FLC/N-PI Integral gain ($1/s$): k_i	0.26
ESPO equivalent input gain ($^\circ \cdot s^3/rad$): b_0	-0.04
ESPO nonlinear coefficient (rad/s): h	0.001
ESPO observer bandwidth: α_0	40
ESPO estimation gain ($1/s$): k_{01}	1.2×10^2
ESPO estimation gain ($1/s^2$): k_{02}	4.8×10^3
ESPO estimation gain ($1/s^3$): k_{03}	6.4×10^4

5.1. Simplified Two-mass Wind Turbine Model

5.1.1. Step Wind Speed Test

The pitch angle controller is designed to maintain the rotor speed under wind disturbance. The performance of the three controllers obtained under different step wind disturbance is shown in Figure 4, which is simulated on the simplified two-mass model. When wind speed is increased in steps, it is clear that the PI controller (dotted line) cannot provide consistently optimal dynamic performance when wind speed changes. The GSPI controller (dashed line) with the entire-region optimal gains can eliminate the effect of the shift of operating points caused by the change of wind speed. The N-PI (solid line) provides better transient response with smaller overshoot and faster settling time, over the whole operation range.

The performance of the ESPO in N-PI is given in Figure 5. Note that the observer needs a short period to track the variation of operating point, it will have transient error under step wind, but will eliminate to zero in a short time

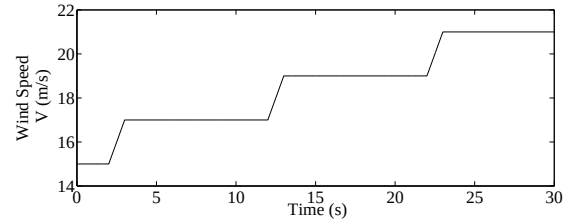

(a)

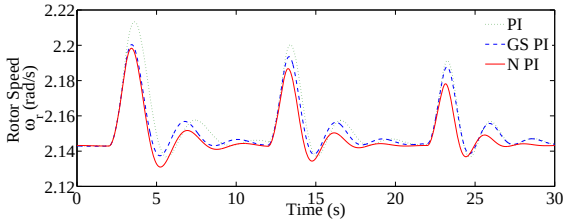

(b)

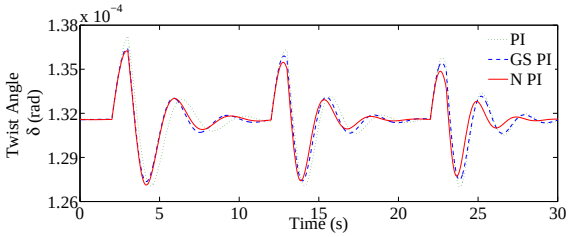

(c)

Figure 4: Response of PI, GSPI and N-PI under step wind test. (a) wind speed, (b) rotor speed, (c) drive train shaft twist angle.

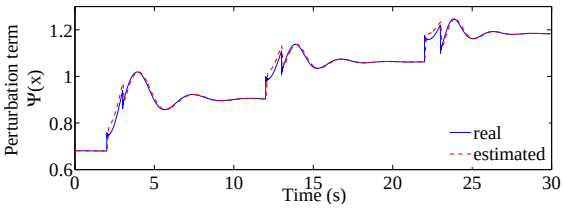

(a)

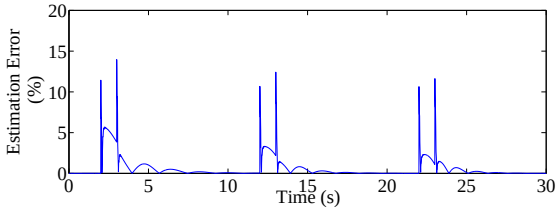

(b)

Figure 5: Perturbation estimation result under step wind speed. a) Real and estimated perturbation comparison; b) Estimation error in percentage.

period. There is no steady-state error between the real perturbation and the estimated value.

Furthermore, dynamic response under step wind speed change from 12 m/s to 24 m/s are compared in terms of settling time, overshoot and ITAE for different controllers. As shown in Figure 6, it can be found that the N-PI has about 18% less settling time, 15% less overshoot, and 20% less ITAE value than the other two when the wind speed above 16 m/s. At lower wind speed, the N-PI performs better than the PI but no obvious improvement than the GSPI. Overall, the N-PI has the best performance with the least ITAE value among the three controllers.

5.1.2. Random Wind Speed Test

The simulation results under random wind with 18 m/s mean speed and 15% turbulence intensity are presented in Figure 7, which contains wind speed, response of rotor speed, and drive train shaft twist angle. All controllers control the pitch angle and the generator torque is held as a constant in its rated value. The control performances are compared under cases with combination of

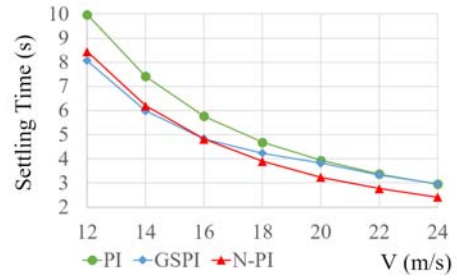

(a)

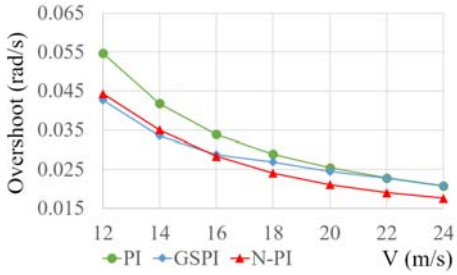

(b)

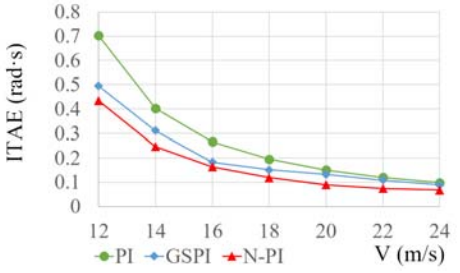

(c)

Figure 6: Performance comparison in metrics of: (a) settling time (s), (b) overshoot (rad/s), and (c) ITAE (rad·s) under step change wind speed.

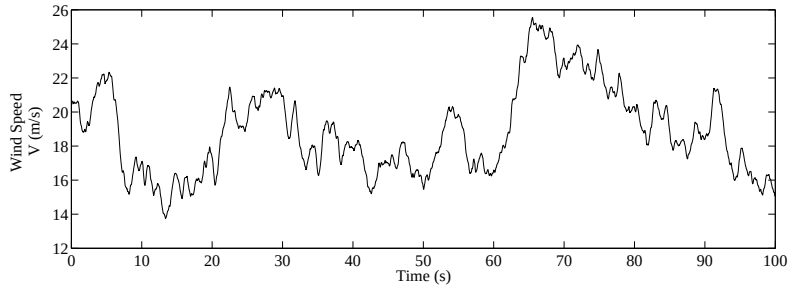

(a)

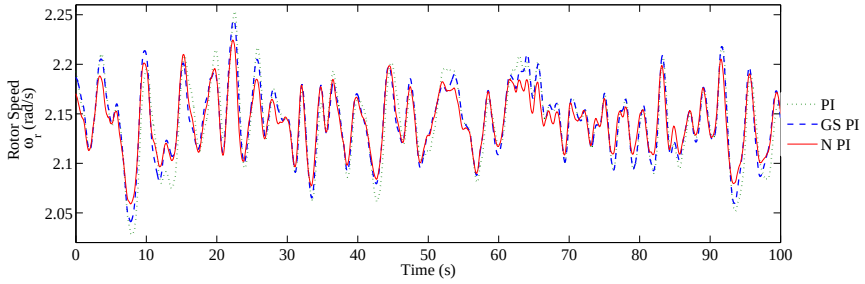

(b)

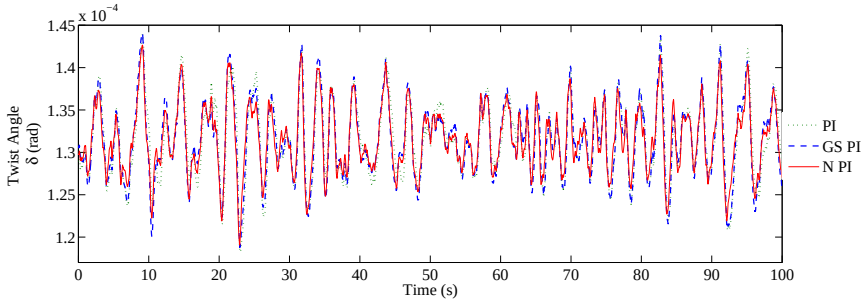

(c)

Figure 7: Response of N-PI compared with PI and GSPI under random wind speed. (a) Random wind speed, (b) rotor speed, (c) drive train shaft twist angle.

different mean wind speed and turbulence intensity, based on the RMS value of the regulation error of the following four dynamic variables: the rotor speed ω_r for the control performance, the twist angle δ as the second control objective, the actuator usage in terms of the pitch acceleration $\dot{\beta}$, and the controller output change rate $\dot{\beta}_r$. Their performances are presented using bar chart in Figure 8. The PI controller performs worst under the random wind speed as shown in the comparison bar charts. This is because that the PI controller is a linear controller with its control gain is optimized at one operation point, while the other three controllers are nonlinear controllers whose control gains are suitable for the whole wind speed region, based on the cancellation of nonlinearities or gain scheduled technique.

On the other hand, the GSPI gain pairs are switching rapidly under the random wind speed. Its entire control performance is not as good as the FLC and the N-PI. Due to the system model and parameters are known accurately in simulation, the FLC has absolutely the best performance among the four controllers. N-PI performs as good as FLC, but the perturbation observer has a small time delay and estimation error by the ESPO estimation before compensate the real ones. The rotor speed regulation error of N-PI is 20% less than the PI controller and 10% less than the GSPI. The reduction of twist angle change is 12% better than the PI and GSPI. In addition, the actuator usage of N-PI is 4% less than that of GSPI and 9% less than that of FLC, in terms of the pitch change rate and control output acceleration.

The estimation performance of the linear ESPO in the N-PI controller is shown in Figure 9, whose average estimation error is around 7.5%.

Due to the high change rate of the random wind speed with high turbulence, the estimated perturbation from ESPO should be filtered before used to compensate the real perturbation. Moreover, the N-PI controller using a nonlinear ESPO is compared a N-PI with a linear ESPO. As the observer gains of both ESPOs are chosen to be far greater than the upper bound of the time derivative of perturbation, there is no obvious improvement obtained by the nonlinear ESPO. Thus this paper uses a high-gain linear ESPO for perturbation estimation [17].

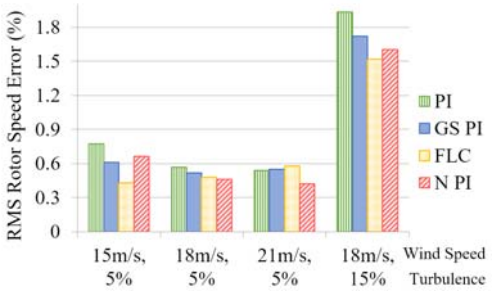

(a)

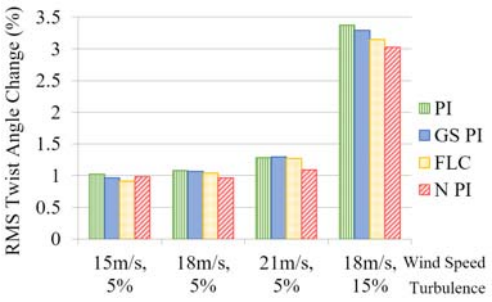

(b)

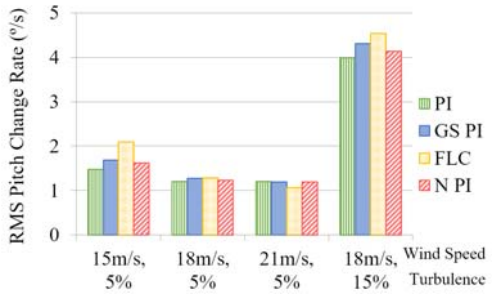

(c)

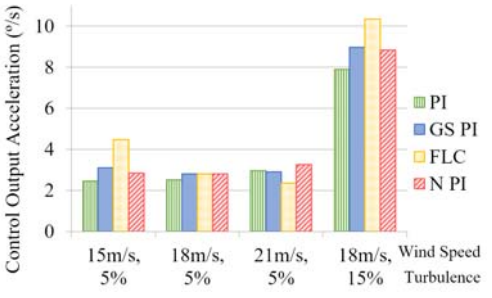

(d)

Figure 8: Performance comparison for PI, GSPI, FLC and N-PI under random wind speed with different mean value (m/s) and turbulence intensity (%). (a) RMS Rotor Speed Error; (b) RMS Twist Angle Change; (c) RMS Pitch Actuator Usage; (d) RMS Controller Output Acceleration.

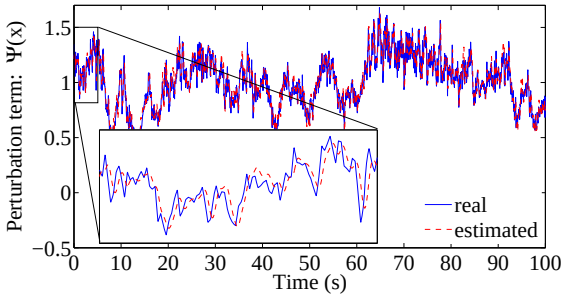

(a)

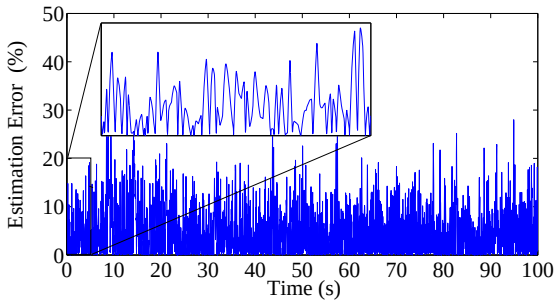

(b)

Figure 9: Perturbation estimation result under random wind speed. a) Real and estimated perturbation comparison; b) Estimation error in percentage.

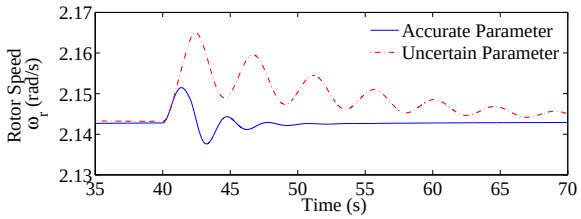

(a) FLC

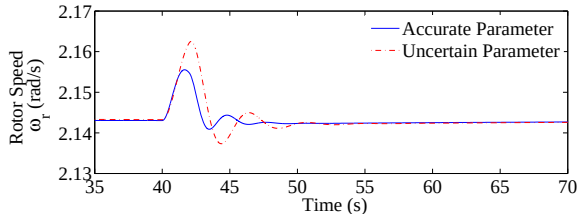

(b) N-PI

Figure 10: Dynamic response comparison under the power coefficient change to 70% its rated value. (a) Dynamic response of FLC; (b) Dynamic response of N-PI.

The proposed N-PI pitch controller has better control performance in the whole wind speed region, especially at high turbulence intensity. Moreover, to extend the service life of equipment, high actuator usage should be avoided in practise. The GSPI requires to tune several set of gains around several operating points, while the N-PI only needs to tune one pair of gains of PI the whole wind speed region, which make it be much easier to comprise the control performance and the actuator usage.

5.1.3. Robustness of Model Uncertainties

When the accurate system model is available, the FLC provides the best results. However, in practical application, there are many model uncertainties, such as air density change caused by different weather condition, dust effect [33], and ice accretion [34][35], which will affect the aerodynamic power coefficient of the wind turbine. Figure 10 shows the dynamic response when the power coefficient is reduced to 70% of its rated value. As the FLC requires an accurate model and parameters, it cannot maintain the rated rotor speed. As the N-PI based controller do not need the accurate system model and can compensate

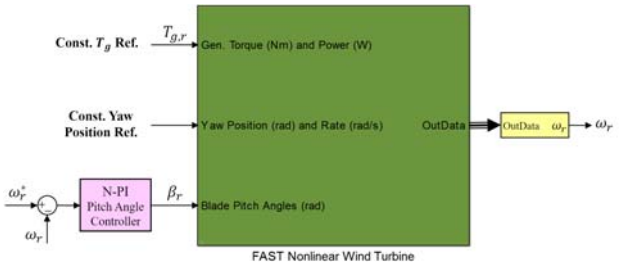

Figure 11: Configuration of test N-PI pitch angle controller using FAST.

the perturbation caused by the variation of system model uncertainties, it can provide much better and robust response. The PI and GSPI can also provide similar robust performance than the N-PI and their results are not presented.

5.2. Validation on FAST Simulator

As the two-mass model is a simplified wind turbine model that neglects many dynamic behavior, the N-PI controller is also validated on a more detailed model, the Fatigue, Aerodynamics, Structures, and Turbulence (FAST) model, which is capable of predicting both the extreme and fatigue loads of two and three-bladed horizontal-axis wind turbines and suitable for verify and test of wind turbine control. Figure 11 shows the configuration of the N-PI and the FAST in Simulink.

As suggested in the FAST user manual, the FAST model does not include the pitch angle actuator dynamics and the blade base can rotate to the reference angle without any delay. An additional actuator dynamic block is added to regulate the pitch angle. Furthermore, the FAST model has no direct output of the twist angle value like in the two-mass model, as it uses a full flexible dynamic model with segmented elastic model in the entire drive train shaft. The low speed shaft damage equivalent load (LSS DEL) is used to display the equivalent performance of the twist angle of the drive train shaft.

In the simulation on FAST model, RMS value of the following three variables are used to compare the controller performance: the rotor speed regulation error, and the pitch acceleration of the pitch angle (in °/s). The dynamic responses under random wind input with 18 m/s mean speed and 15% turbulence intensity

is presented in Figure 12. Comparing with the response of two mass model, the FAST simulation result includes many authentic dynamics and high frequency noise. The comparison performs in the bar chart shows that the N-PI has the rotor speed regulation error 25%∼30% less than the PI and 5%∼15% less than the GSPI as shown in Figure 13(a). And in the RMS of LSS DEL, the N-PI has approximate 7% less than both the PI and the GSPI as shown in Figure 13(b).

In the FAST simulation, the pitch angle response time constant depends on many conditions, such as wind speed at different height, yaw angle, and tower shadow, etc. Therefore, the pitch angle control response in FAST simulation is worse under higher wind speed and greater turbulence intensity as shown in Figure 13(c). Nevertheless, the results under both low and high turbulence wind show that the N-PI controller has approximate 13% less actuator usage than the GSPI and gets about 10% better performance, and it has approximate 6% more actuator usage to get a 28% improvements comparing with PI controller in wind turbine pitch control.

6. Conclusion

A Nonlinear PI (N-PI) pitch angle controller has been designed to regulate the wind turbine to capture the rated wind power when the wind speed exceeds the rated value. Based on the two-mass nonlinear wind turbine model, an extended-order state and perturbation observer is designed to estimate the unknown and time-varying nonlinearities and external disturbances. The estimated perturbation dynamic is used to compensate the real unknown dynamics and a PI type controller is designed for the linearized system. Only one set of PI parameters are needed to be tuned for covering the whole operation region. The N-PI avoids the requirement of tuning and switching of controller gains in GSPI and the requirement of accurate system model in the feedback linearization control. The proposed N-PI pitch angle controller is verified on the two-mass simplified model and then the detailed FAST simulator under step and random wind speed tests. Simulation results show that the N-PI based pitch

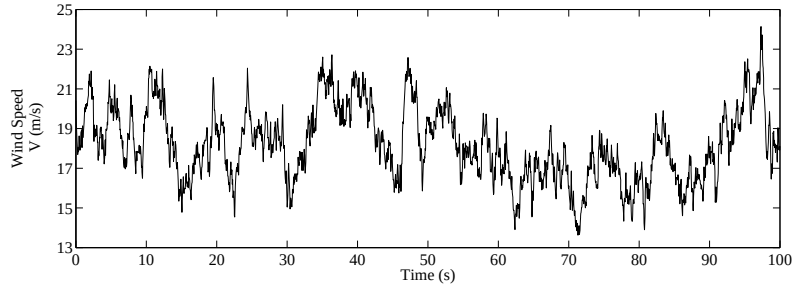

(a)

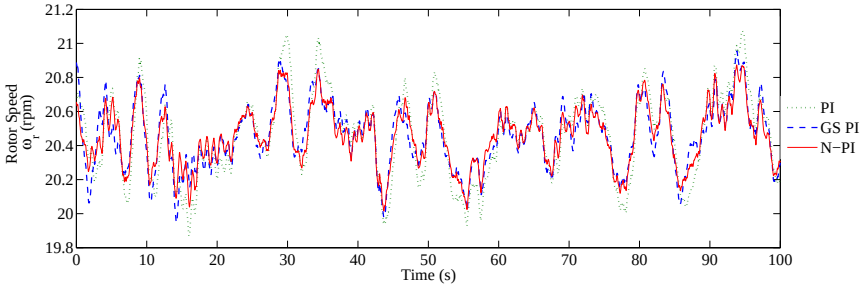

(b)

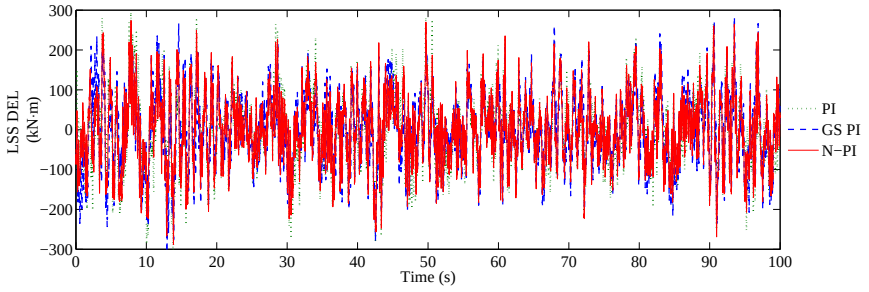

(c)

Figure 12: Simulation verification result on FAST model. (a) wind speed, (b) rotor speed, (c) LSS DEL.

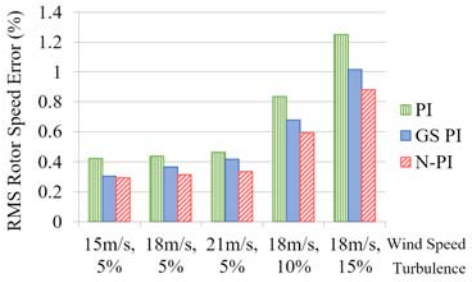

(a)

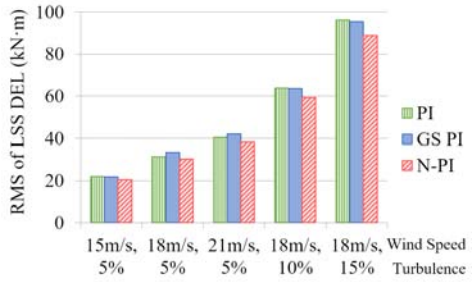

(b)

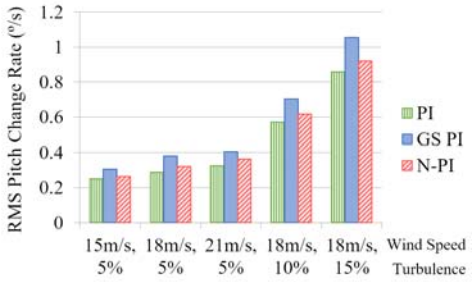

(c)

Figure 13: Performance comparisons of PI, GSPI and N-PI controllers using FAST simulator under different wind input: (a) RMS rotor speed error; (b) RMS LSS DEL; (c) RMS pitch change rate.

angle controller performs better in constant power regulation and drive-train stress minimization, with less actuator usage comparing with the conventional PI and gain-scheduled PI controllers, and better robustness than FLC in the model uncertainties.

References

[1] F. D. Bianchi, H. De Battista, R. J. Mantz, Wind turbine control systems: principles, modelling and gain scheduling design, Springer Science & Business Media, 2006.

[2] B. Boukhezzar, H. Siguerdidjane, Comparison between linear and nonlinear control strategies for variable speed wind turbines, Control Engineering Practice 18 (12) (2010) 1357–1368.

[3] L. Y. Pao, K. E. Johnson, Control of wind turbines, Control Systems, IEEE 31 (2) (2011) 44–62.

[4] M. H. Hansen, A. D. Hansen, T. J. Larsen, S. Øye, P. Sørensen, P. Fuglsang, Control design for a pitch-regulated, variable speed wind turbine, 2005.

[5] B. Beltran, T. Ahmed-Ali, M. E. H. Benbouzid, Sliding mode power control of variable-speed wind energy conversion systems, Energy Conversion, IEEE Transactions on 23 (2) (2008) 551–558.

[6] A. Kumar, K. Stol, Simulating feedback linearization control of wind turbines using high-order models, Wind Energy 13 (5) (2010) 419–432.

[7] H. Camblong, Digital robust control of a variable speed pitch regulated wind turbine for above rated wind speeds, Control Engineering Practice 16 (8) (2008) 946–958.

[8] A. S. Yilmaz, Z. Özer, Pitch angle control in wind turbines above the rated wind speed by multi-layer perceptron and radial basis function neural networks, Expert Systems with Applications 36 (6) (2009) 9767–9775.

[9] D. Schlipf, D. J. Schlipf, M. Kühn, Nonlinear model predictive control of wind turbines using LIDAR, Wind Energy 16 (7) (2013) 1107–1129.

[10] D. Leith, W. Leithead, Implementation of wind turbine controllers, International Journal of Control 66 (3) (1997) 349–380.

[11] K.-H. Kim, M.-J. Youn, A nonlinear speed control for a PM synchronous motor using a simple disturbance estimation technique, Industrial Electronics, IEEE Transactions on 49 (3) (2002) 524–535.

[12] J. Han, From PID to active disturbance rejection control, Industrial Electronics, IEEE transactions on 56 (3) (2009) 900–906.

[13] W. Zhou, S. Shao, Z. Gao, A stability study of the active disturbance rejection control problem by a singular perturbation approach, Applied Mathematical Sciences 3 (10) (2009) 491–508.

[14] X. Chen, S. Komada, T. Fukuda, Design of a nonlinear disturbance observer, Industrial Electronics, IEEE Transactions on 47 (2) (2000) 429–437.

[15] L. Jiang, Q. Wu, J. Wang, C. Zhang, X. Zhou, Robust observer-based nonlinear control of multimachine power systems, in: Generation, Transmission and Distribution, IEE Proceedings-, Vol. 148, IET, 2001, pp. 623–631.

[16] S. Li, Z. Liu, Adaptive speed control for permanent-magnet synchronous motor system with variations of load inertia, Industrial Electronics, IEEE Transactions on 56 (8) (2009) 3050–3059.

[17] L. Jiang, Q. Wu, Nonlinear adaptive control via sliding-mode state and perturbation observer, IEE Proceedings-Control Theory and Applications 149 (4) (2002) 269–277.

[18] E. Kim, A fuzzy disturbance observer and its application to control, Fuzzy Systems, IEEE Transactions on 10 (1) (2002) 77–84.

[19] J.-S. Ko, B.-M. Han, Precision position control of PMSM using neural network disturbance observer on forced nominal plant, in: Mechatronics, 2006 IEEE International Conference on, IEEE, 2006, pp. 316–320.

[20] W.-H. Chen, D. J. Ballance, P. J. Gawthrop, J. J. Gribble, J. O. Reilly, A nonlinear disturbance observer for two link robotic manipulators, in: Decision and Control, 1999. Proceedings of the 38th IEEE Conference on, Vol. 4, IEEE, 1999, pp. 3410–3415.

[21] J. Chen, L. Jiang, W. Yao, Q. Wu, Perturbation estimation based nonlinear adaptive control of a full-rated converter wind turbine for fault ride-through capability enhancement, Power Systems, IEEE Transactions on 29 (6) (2014) 2733–2743.

[22] Z. Gao, Active disturbance rejection control: a paradigm shift in feedback control system design, in: American Control Conference, 2006, IEEE, 2006, pp. 7–pp.

[23] D. Patel, L. Zhao, Active disturbance rejection control of doubly-fed induction generator during voltage dip, in: Proc. ESA Annual Meeting on Electrostatics, 2010, p. 2.

[24] J. M. Jonkman, M. L. Buhl Jr, FAST user's guide, National Renewable Energy Laboratory, Golden, CO, Technical Report No. NREL/EL-500-38230.

[25] B. Boukhezzar, H. Siguerdidjane, Nonlinear control of a variable-speed wind turbine using a two-mass model, Energy Conversion, IEEE Transactions on 26 (1) (2011) 149–162.

[26] S. C. Thomsen, Nonlinear control of a wind turbine, Ph.D. thesis, Technical University of Denmark, DTU, DK-2800 Kgs. Lyngby, Denmark (2006).

[27] W. M. Korani, H. T. Dorrah, H. M. Emara, Bacterial foraging oriented by particle swarm optimization strategy for PID tuning, in: Computational Intelligence in Robotics and Automation (CIRA), 2009 IEEE International Symposium on, IEEE, 2009, pp. 445–450.

[28] M. I. Solihin, L. F. Tack, M. L. Kean, Tuning of PID controller using particle swarm optimization (PSO), International Journal on Advanced Science, Engineering and Information Technology 1 (4) (2011) 458–461.

[29] E. B. Muhando, T. Senjyu, N. Urasaki, A. Yona, H. Kinjo, T. Funabashi, Gain scheduling control of variable speed WTG under widely varying turbulence loading, Renewable Energy 32 (14) (2007) 2407–2423.

[30] E. B. Muhando, T. Senjyu, A. Uehara, T. Funabashi, Gain-scheduled control for wecs via LMI techniques and parametrically dependent feedback part ii: controller design and implementation, Industrial Electronics, IEEE Transactions on 58 (1) (2011) 57–65.

[31] T. L. Van, T. H. Nguyen, D.-C. Lee, Advanced pitch angle control based on fuzzy logic for variable-speed wind turbine systems, Energy Conversion, IEEE Transactions on 30 (2) (2015) 578–587.

[32] B. J. Jonkman, TurbSim user's guide: version 1.50, National Renewable Energy Laboratory Golden, CO, USA, 2009.

[33] M. G. Khalfallah, A. M. Koliub, Effect of dust on the performance of wind turbines, Desalination 209 (1) (2007) 209–220.

[34] L. Makkonen, T. Laakso, M. Marjaniemi, K. Finstad, Modelling and prevention of ice accretion on wind turbines, Wind Engineering 25 (1) (2001) 3–21.

[35] S. Saleh, R. Ahshan, C. Moloney, Wavelet-based signal processing method for detecting ice accretion on wind turbines, Sustainable Energy, IEEE Transactions on 3 (3) (2012) 585–597.